ISSN 0006-2979, Biochemistry (Moscow), 2024, Vol. 89, No. 7, pp. 1202-1210 © The Author(s) 2024. This article is an open access publication.

Mechanism of PARP1 Elongation Reaction Revealed by Molecular Modeling

Sergey V. Pushkarev[1], Evgeny M. Kirilin[2,a], Vytas K. Švedas[1,3], and Dmitry K. Nilov[3,b]*

[1]*Faculty of Bioengineering and Bioinformatics, Lomonosov Moscow State University, 119234 Moscow, Russia*

[2]*Abu Dhabi, United Arab Emirates*

[3]*Lomonosov Moscow State University, Belozersky Institute of Physicochemical Biology, 119992 Moscow, Russia*

[a]*e-mail: e.kirilin@gmail.com* [b]*e-mail: nilovdm@gmail.com*

Received April 15, 2024
Revised June 6, 2024
Accepted June 8, 2024

Abstract—Poly(ADP-ribose) polymerase 1 (PARP1) plays a major role in the DNA damage repair and transcriptional regulation, and is targeted by a number of clinical inhibitors. Despite this, catalytic mechanism of PARP1 remains largely underexplored because of the complex substrate/product structure. Using molecular modeling and metadynamics simulations we have described in detail elongation of poly(ADP-ribose) chain in the PARP1 active site. It was shown that elongation reaction proceeds via the S_N1-like mechanism involving formation of the intermediate furanosyl oxocarbenium ion. Intriguingly, nucleophilic $2'_A$-OH group of the acceptor substrate can be activated by the general base Glu988 not directly but through the proton relay system including the adjacent $3'_A$-OH group.

DOI: 10.1134/S0006297924070046

Keywords: Poly(ADP-ribose) polymerase 1, PARP1, ADP-ribosylation, reaction mechanism, oxocarbenium ion, molecular modeling, metadynamics

INTRODUCTION

Poly(ADP-ribose) polymerase 1 enzyme (PARP1) plays an important role in regulating gene expression and maintaining genome integrity. PARP1 is activated under conditions of stress and synthesizes a negatively charged polymer, poly(ADP-ribose) (PAR), that performs signaling functions [1-6]. PARP1 is the most abundant of the PARP family members (PARPs 1-4, tankyrases 1 and 2, PARPs 6-16) and accounts for approximately 90% of PARP catalytic activity [7-9]. Pathogenesis of the diseases of cardiovascular, nervous, immune, respiratory, and other body systems is often associated with PARP1 activation and PAR synthesis [10-13]. Furthermore, preclinical data on the PARP1's involvement in DNA repair led to the development of a series of novel anticancer inhibitors (including olaparib, rucaparib, niraparib, etc.) [14-17].

PARP1 utilizes NAD^+ as a donor of ADP-ribose units, releasing nicotinamide as a by-product. PAR synthesis involves three ADP-ribosylation reactions: (i) initiation (attachment of the first ADP-ribose unit to an acceptor protein), (ii) elongation, and (iii) branching (Fig. 1) [18-21]. In the elongation reaction, the *O*-glycosidic bond is formed between the adenine ribose of the terminal PAR residue and nicotinamide ribose of the metabolized NAD^+, with the $2'_A$-OH group acting as an attacking nucleophile. In the branching reaction, the bond is formed between two nicotinamide ribose rings, with $2'_N$-OH acting as a nucleophile (subscripts A and N denote adenine and nicotinamide ribose, respectively). Formation of the negatively charged PAR polymers (up to 200 units in size) results in modulation of chromatin structure and recruitment of a number of cellular proteins [22]. In particular, activity of PARP1

Abbreviations: MD, molecular dynamics; MM, molecular mechanics; PAR, poly(ADP-ribose); PARP1, poly(ADP-ribose) polymerase 1; QM, quantum mechanics.

* To whom correspondence should be addressed.

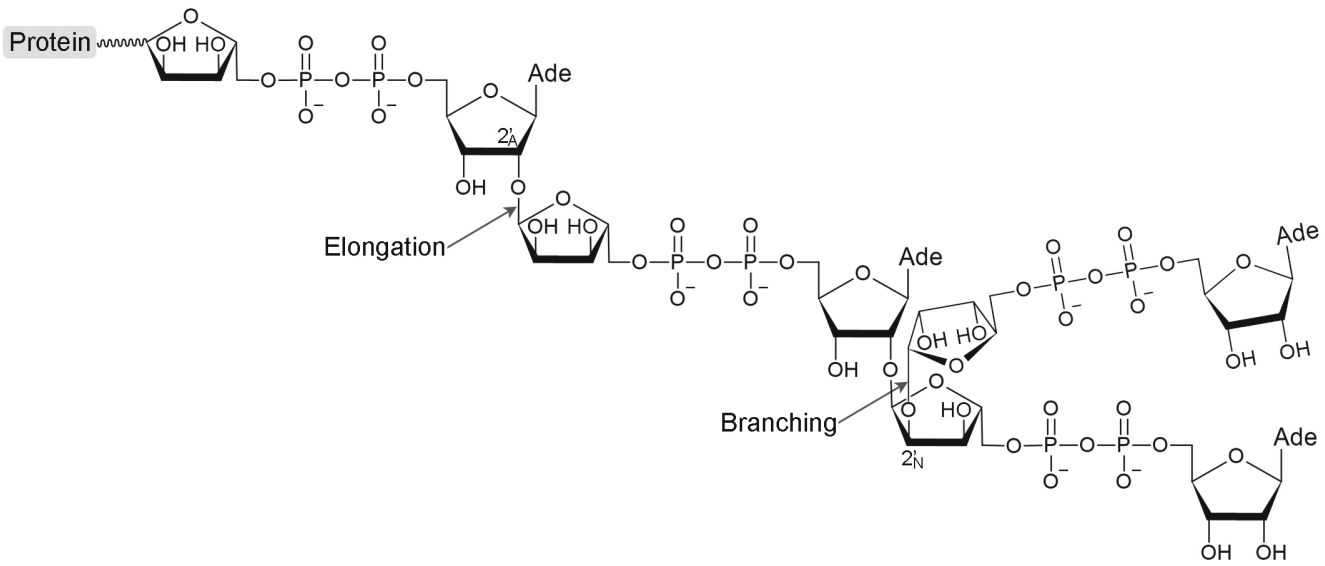

Fig. 1. Chemical structure of PAR composed of ADP-ribose units. Branches are formed every 40-50 units.

at the sites of DNA damage recruits base excision repair proteins XRCC1, DNA polymerase β, and DNA ligase III [23, 24].

Despite its biological significance, catalytic mechanism of PAR synthesis remains underexplored because of the complex substrate/product structure. Some assumptions on the PAR and NAD^+ binding can be made based on the crystal structure of the complexes of PARP1 with inactive substrate mimics [18, 25, 26]. The Glu988 residue in the active site is critical for polymer growth and likely provides the required orientation of PAR and NAD^+ by forming hydrogen bonds with their $3'_A$-OH and $2'_N$-OH groups [18, 25, 27, 28]. Some authors consider that Glu988 also forms a hydrogen bond with the $2'_A$-OH group of PAR and acts as a proton acceptor upon nucleophilic attack by the S_N2 mechanism [18, 27]. However, in our molecular dynamics (MD) simulation of the enzyme–substrate complex with terminal fragment of PAR and NAD^+ we failed to observe direct interaction between the Glu988 and $2'_A$-OH as well as reactive in-line configuration of the $O2'_A$, $C1'_N$, and $N1_N$ atoms, typical for S_N2 [29]. The present paper is a further attempt to provide details concerning PARP1 catalysis through molecular modeling and metadynamics simulations. We describe the possible S_N1-like mechanism for the elongation reaction involving formation of an intermediate oxocarbenium ion.

MATERIALS AND METHODS

Starting model of the PARP1 enzyme-substrate complex was constructed based on the catalytic domain coordinates extracted from the 4dqy crystal structure (residues 662-1011) [30]. N- and C-terminal ends of the protein were capped with ACE (acetyl) and NME (*N*-methylamide) groups, respectively. Coordinates of NAD^+ were transferred from the 6bhv structure [26]. Coordinates of an ADP moiety as a terminal PAR fragment were transferred from the 1a26 structure [18]; its diphosphate chain was capped with a methyl group (Fig. S1 in the Online Resource 1).

Next, the model was optimized using AmberTools20 and Amber20 [31-33] installed on the Lomonosov-2 supercomputer [34]. The protein molecule was described with the *ff14SB* force field [35]. The NAD^+ molecule was described with parameters from the Amber Parameter Database (http://amber.manchester.ac.uk) [36, 37]. Parameters for the methyl-ADP molecule were derived as follows. Force constants, equilibrium bond lengths/angle values, and van der Waals parameters were taken from the NAD^+ parameter set. Partial atomic charges were taken from the NAD^+ set except for the methoxy group. Charges for this group were determined using the R.E.D.-III.5 and RESP programs [38, 39], as shown in Fig. S2 in the Online Resource 1. Hydrogen atoms were added to the protein structure considering ionization properties of amino acid residues, and then it was surrounded by a layer of TIP3P water (12 Å).

Energy minimization included two stages: the first one with positional restraints on heavy atoms of the protein and substrates (2500 steepest descent steps + 2500 conjugate gradient steps), and the second one without restraints (5000 steepest descent steps + 5000 conjugate gradient steps). The obtained system was heated up from 0 to 300 K with positional restraints on the protein and substrate atoms (1000 ps, constant volume) and equilibrated at 300 K (1000 ps, constant pressure); time step was 0.002 ps. Finally, a 100 ns trajectory of the equilibrium MD simulation was calculated. All protocols are described in detail in our

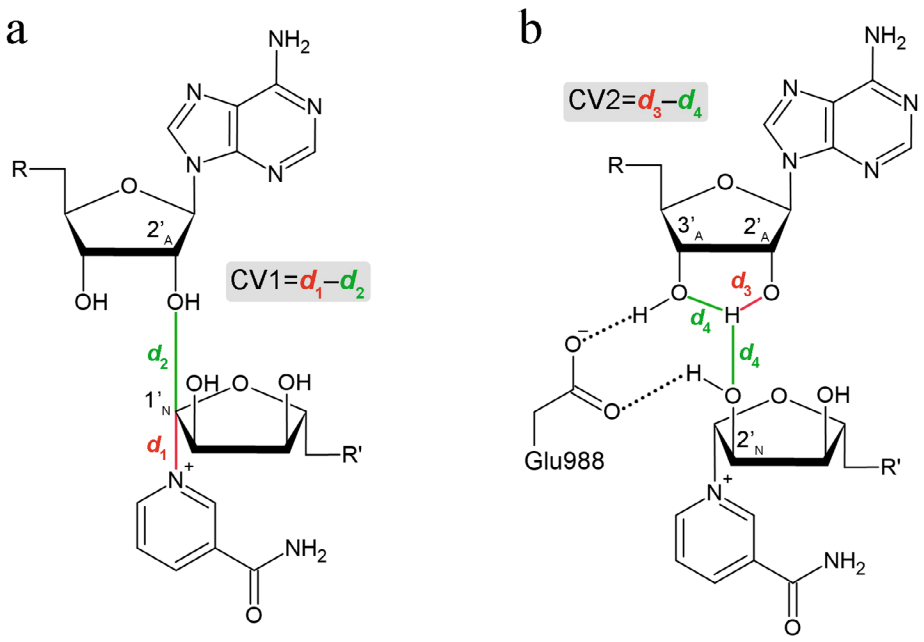

Fig. 2. Collective variables used for metadynamics simulations. a) CV1 describes nucleophilic substitution at the C1′$_N$ atom. b) CV2 describes deprotonation of the nucleophilic 2′$_A$-OH group. This group is activated by Glu988, and the corresponding proton relay system could include either the 3′$_A$-OH (system A) or 2′$_N$-OH (system B) group.

previous work [40]. The simulation trajectories were analyzed using cpptraj 5.1.0 [41] and VMD 1.9 [42].

To perform metadynamics calculations, 4 frames were selected from the equilibrium MD trajectory in which positions of the substrates were close to the reactive configuration. Each selected frame was then simulated using a hybrid quantum mechanics/molecular mechanics (QM/MM) functionality in Amber20 [43]; detailed protocols are given in Table S1 in the Online Resource 1. The QM region included essential parts of the substrates and of Lys903 and Glu988 residues, which were treated using the PM6-D semi-empirical Hamiltonian [44, 45], and the MM region included the remaining atoms of the system (Fig. S3 in the Online Resource 1). Prior to metadynamics, 25 ps simulations with 0.001-ps time steps were carried out to adjust structures of the active site after switching from the MM to QM/MM approximation. Next, well-tempered metadynamics implemented in Plumed 2.6.2 [46-50] was used to explore free energy surface of the PARP1-catalyzed elongation reaction. Free energy landscape was reconstructed by 8 simulations (2 for each starting structure) run in parallel with shared metadynamics potential (so-called “walkers”) [51]. Duration of each simulation was 300 ps, time step was 0.0005 ps.

The first collective variable (CV1) was defined as d_1-d_2, where d_1 – distance between the C1′$_N$ and N1$_N$ atoms, and d_2 – distance between the O2′$_A$ and C1′$_N$ atoms (Fig. 2a). The second collective variable (CV2) was defined as d_3-d_4, where d_3 – distance between the O2′$_A$ and O2′$_A$:H atoms, and d_4 – distance between the O2′$_A$:H atom and either the O3′$_A$ or O2′$_N$ atom (Fig. 2b). CV1 describes nucleophilic substitution at the C1′$_N$ atom, and CV2 – deprotonation of the nucleophilic 2′$_A$-OH group. Gaussian potentials of an initial height of 6 kJ/mol and width of 0.1 Å (CV1) and 0.075 Å (CV2) were added every 100 simulation steps, bias factor was set to 16. Upper and lower walls were applied to d_1, d_2, d_3, and d_4 (to limit exploration in the CV1/CV2 space), as well as to some other distances to prevent unwanted proton transfer scenarios (e.g., transfer between O2′$_A$ and O2′$_N$ in system A, or between O2′$_A$ and O3′$_A$ in system B). Gaussian potentials were summed with metadynminer 0.1.7 (“fes2” function) [52], minimum energy paths were calculated using the nudged elastic band method [53].

RESULTS

Elongation of PAR polymers is the most common reaction catalyzed by PARP1. Two substrates are required for elongation activity: NAD$^+$ (ADP-ribose donor) and terminal PAR fragment (ADP-ribose acceptor). We have decided to use methyl-ADP molecule as a structural analogue of the acceptor substrate terminus in molecular modeling experiments. A 100-ns MD simulation of the PARP1 enzyme-substrate complex demonstrated that NAD$^+$ forms two hydrogen bonds with Gly863 and π-stacking with Tyr907, which confirms the results of previous studies [25, 29]. The catalytic Glu988 residue forms hydrogen bonds with the 2′$_N$-OH group of NAD$^+$ and 3′$_A$-OH group of methyl-ADP, providing reactive orientation of the substrates.

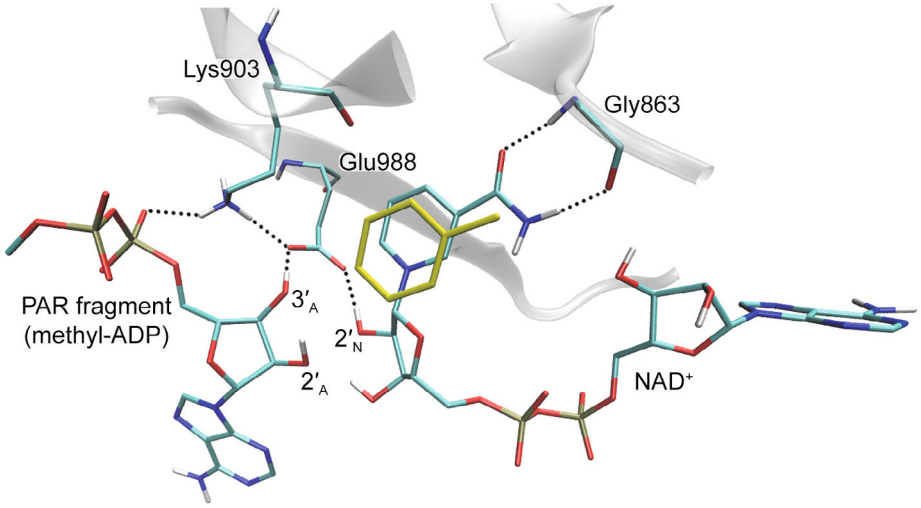

Fig. 3. Important molecular interactions observed in the modeled enzyme–substrate complex of PARP1. Hydrogen bonds of Gly863, Lys903, and Glu988 are shown as dotted lines. Phenyl group of Tyr907 forming π-stacking is shown in yellow. For clarity, non-polar hydrogen atoms are omitted.

The neighboring Lys903 residue forms hydrogen bonds with both Glu988 side chain (stabilizing its conformation) and diphosphate moiety of methyl-ADP (Fig. 3).

Nucleophilic 2′$_A$-OH group of the acceptor substrate is presumably activated by the Glu988 carboxyl group [18, 27]. However, according to the MD modeling data, these groups do not interact with each other directly (Fig. 3). We therefore considered two possible proton relay pathways for further metadynamics simulations: in system A proton transfer is mediated by the 3′$_A$-OH of the acceptor substrate, and in system B – by the 2′$_N$-OH of the donor substrate (Fig. 2b).

QM/MM metadynamics allowed us to reconstruct 2D free-energy landscapes of the PARP1-catalyzed elongation reaction, in which CV1 describes nucleophilic substitution at the C1′$_N$ atom, and CV2 – deprotonation of the nucleophilic 2′$_A$-OH group (Fig. 4). The energy surfaces demonstrate that in the case of both proton relay systems, A and B, the reaction proceeds via the S_N1-like mechanism: an intermediate (oxocarbenium ion) is formed and next it is attacked by the 2′$_A$-OH group of the acceptor substrate, with concomitant proton transfer to Glu988. It is worth mentioning, however, that the proton transfer is conducted by the 3′$_A$-OH (System A) rather than by 2′$_N$-OH (System B), as indicated by the corresponding free-energy barriers (Fig. 5). Discrepancy in the P (reaction products) energies is likely due to the proton transfer to different oxygen atoms of the Glu988 carboxyl group in systems A and B (see Fig. 2).

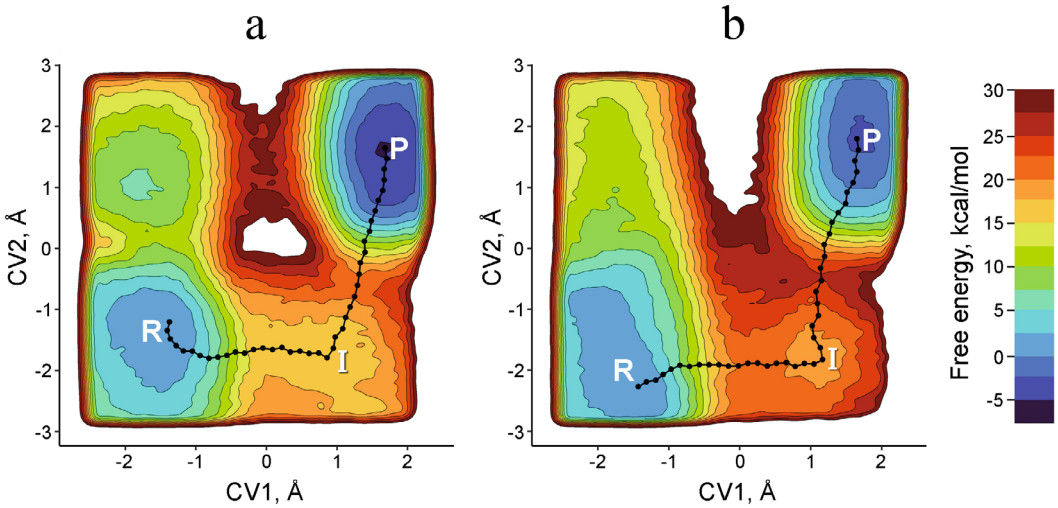

Fig 4. 2D free-energy landscapes of the PARP1-catalyzed elongation reaction. a) Proton relay system A (includes 3′$_A$-OH). b) Proton relay system B (includes 2′$_N$-OH). Collective variable CV1 describes nucleophilic substitution at the C1′$_N$ atom, and CV2 – deprotonation of the nucleophilic 2′$_A$-OH group. An oxocarbenium ion intermediate (I) is formed along the minimum energy pathway between reactants (R) and products (P).

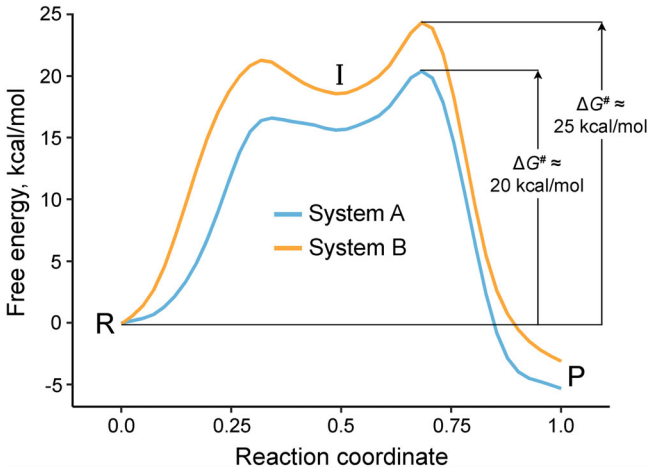

Fig. 5. Comparison of the free energy profiles of elongation reaction reconstructed using proton relay systems A and B (R, reactants; I, intermediate; P, products). The reaction coordinate represents progress along the minimum energy pathways shown in Fig. 4. Calculated errors for R, I, and P states are given in Table S2 in the Online Resource 1.

Figure 6 shows the obtained structures of the reactants, oxocarbenium ion intermediate, and products in system A. The reactants are properly oriented with respect to each other by the Glu988 residue to maintain the reactive conformation (Fig. 6a). The oxocarbenium ion intermediate is formed with the release of nicotinamide and is stabilized due to the negative charge of Glu988. Planar configuration of the reactive center (C1′$_N$ atom) facilitates subsequent nucleophilic attack by the 2′$_A$-OH group (Fig. 6b). A new *O*-glycosidic bond is formed between the adenine ribose and nicotinamide ribose to produce the elongation reaction product; the Glu988 side chain becomes protonated due to the proton transfer from 2′$_A$-OH (Fig. 6c).

DISCUSSION

Metadynamics is a powerful method to investigate free energy landscapes of enzymatic reactions [54-58]. It biases the system evolution by a potential constructed as the sum of Gaussian functions deposited along the trajectory in the collective variable space [46]. The presented metadynamics study describes in detail the PARP1 elongation reaction mechanism, summarized in Fig. 7. It shows attachment of the ADP-ribose unit to the growing PAR chain accompanied with proton transfer to Glu988 via the 3′$_A$-OH group. Formation of the intermediate furanosyl oxocarbenium ion confirms our hypothesis about the S_N1-like mechanism [29]. The main limitation of our methodology is that the acceptor substrate is modeled using the methyl-ADP molecule. The negatively charged PAR polymer may electrostatically contribute to formation of the oxocarbenium ion, whereas methyl-ADP mimics only the terminal PAR unit.

Participation of 3′$_A$-OH in catalysis is consistent with the results of an experimental study of NAD$^+$ analogues lacking hydroxyl groups at positions 3′$_A$ and/or 2′$_A$ [59]. Qualitative analysis (SDS-PAGE/Western blotting with anti-PAR antibodies) showed that absence of the 3′$_A$-OH group leads to the less efficient PAR formation, but not completely prevents the reaction (which points to the existence of an alternative 2′$_N$-OH proton relay system). The preferable proton transfer via 3′$_A$-OH could presumably be explained by a shorter distance between the 2′$_A$-OH and 3′$_A$-OH groups in the enzyme-substrate complex: the distance O2′$_A$ ··· O3′$_A$ calculated from the 100 ns MD trajectory was 2.7 ± 0.1 Å, whereas the distance O2′$_A$ ··· O2′$_N$ was 3.2 ± 0.5 Å. It might be interesting to design NAD$^+$ analogues lacking hydroxyl group at the position 2′$_N$ or at both positions 3′$_A$ and 2′$_N$ to confirm our hypothesis on the proton relay.

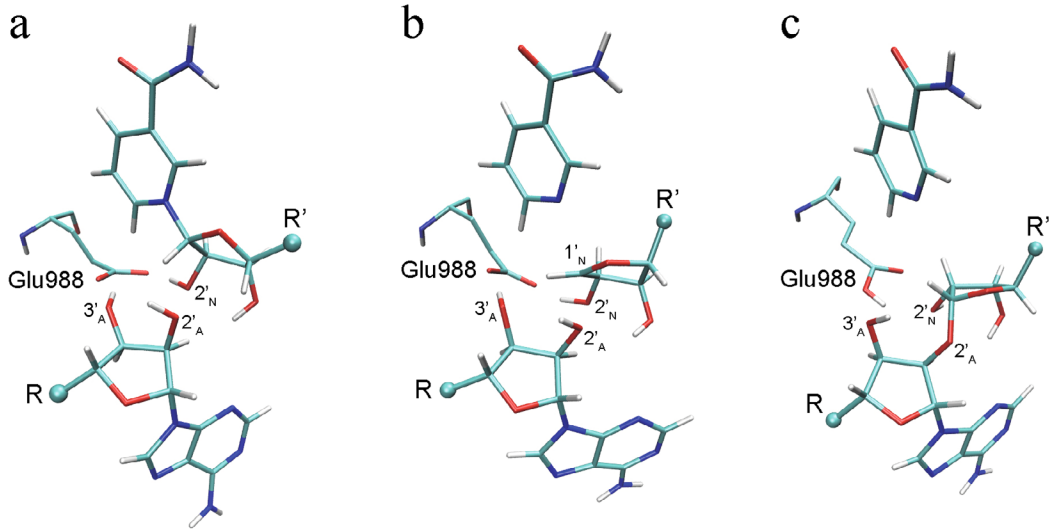

Fig. 6. Structures of reactants (a), oxocarbenium ion intermediate (b), and products (c) obtained from modeling of the PARP1-catalyzed elongation reaction.

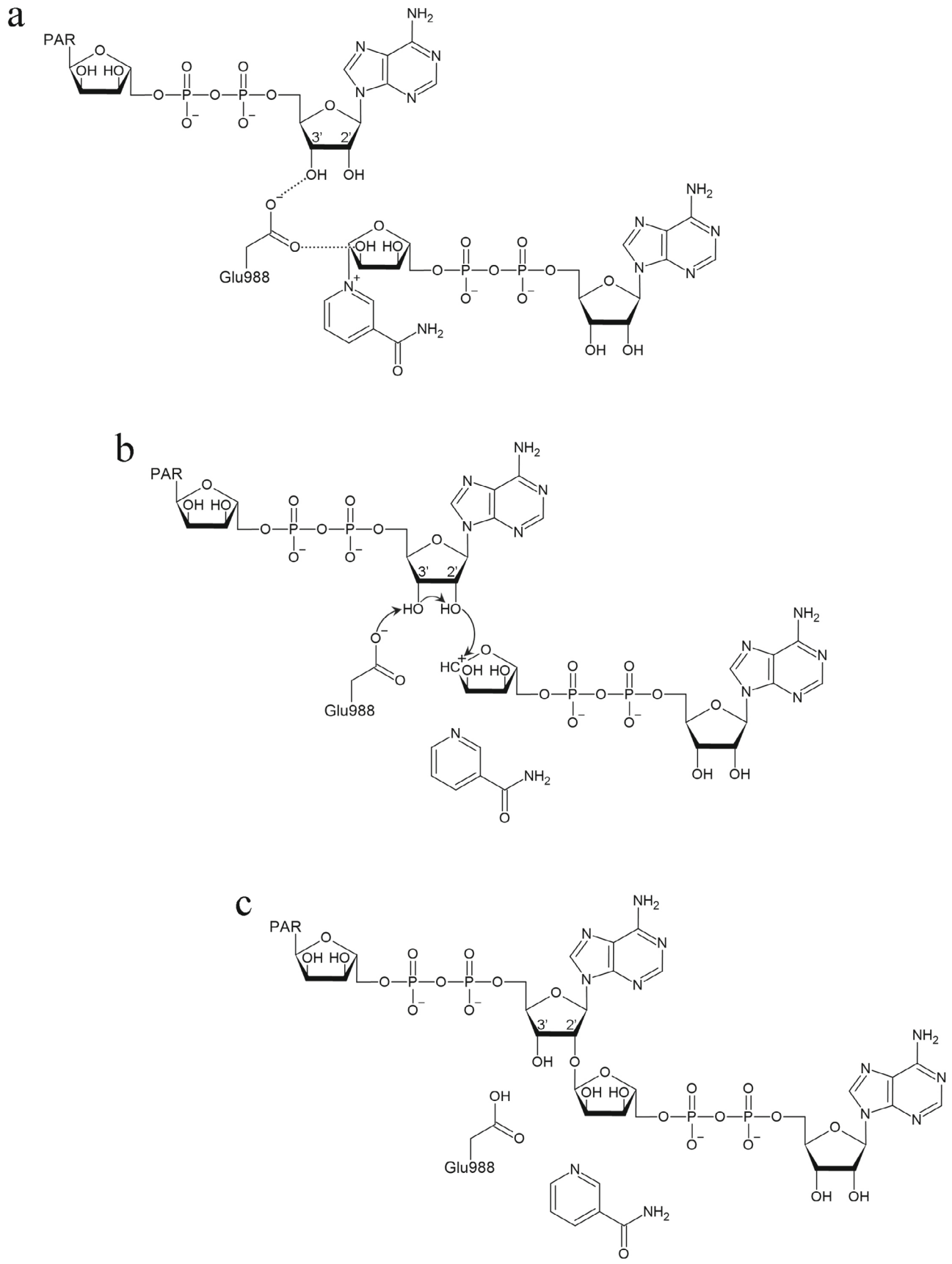

Fig. 7. Proposed S_N1 mechanism of the PARP1 elongation reaction. a) Substrate binding. b) Oxocarbenium ion intermediate. c) Product formation.

Using molecular modeling and metadynamics simulations, we have demonstrated for the first time that the PARP1-catalyzed elongation reaction proceeds via the S_N1-like mechanism involving formation of an intermediate oxocarbenium ion. Intriguingly, our results show that the nucleophilic $2'_A$-OH group of the acceptor substrate (terminal PAR unit) is activated by the general base Glu988 not directly but through the proton relay system including the adjacent $3'_A$-OH group. The findings of this study shed light on the PAR synthesis machinery involving complex polymer substrates and PARP1, a major sensor of DNA damage, and may be used in further design of new PARP1 competitive inhibitors mimicking the substrate and/or oxocarbenium intermediate structure.

Supplementary information. The online version contains supplementary material available at https://doi.org/10.1134/S0006297924070046.

Acknowledgments. The research was carried out using equipment of the shared research facilities of HPC computing resources at Lomonosov Moscow State University.

Contributions. D.K.N. conceptualization and management; S.V.P. and E.M.K. investigation; D.K.N. and S.V.P. writing original draft; V.K.Š. review and editing.

Funding. This study was financially supported by the Russian Science Foundation (project no. 19-74-10072).

Ethics declarations. This work does not contain any studies involving human and animal subjects. The authors of this work declare that they have no conflicts of interest.

REFERENCES

1. Schreiber, V., Dantzer, F., Ame, J. C., and de Murcia, G. (2006) Poly(ADP-ribose): novel functions for an old molecule, *Nat. Rev. Mol. Cell Biol.*, **7**, 517-528, https://doi.org/10.1038/nrm1963.
2. Virág, L., Robaszkiewicz, A., Rodriguez-Vargas, J. M., and Oliver, F. J. (2013) Poly(ADP-ribose) signaling in cell death, *Mol. Aspects Med.*, **34**, 1153-1167, https://doi.org/10.1016/j.mam.2013.01.007.
3. Shilovsky, G. A., Khokhlov, A. N., and Shram, S. I. (2013) The protein poly(ADP-ribosyl)ation system: its role in genome stability and lifespan determination, *Biochemistry (Moscow)*, **78**, 433-444, https://doi.org/10.1134/S0006297913050015.
4. Ryu, K. W., Kim, D. S., and Kraus, W. L. (2015) New facets in the regulation of gene expression by ADP-ribosylation and poly(ADP-ribose) polymerases, *Chem. Rev.*, **115**, 2453-2481, https://doi.org/10.1021/cr5004248.
5. Gupte, R., Liu, Z., and Kraus, W. L. (2017) PARPs and ADP-ribosylation: recent advances linking molecular functions to biological outcomes, *Genes Dev.*, **31**, 101-126, https://doi.org/10.1101/gad.291518.116.
6. Kamaletdinova, T., Fanaei-Kahrani, Z., and Wang, Z. Q. (2019) The enigmatic function of PARP1: from PARylation activity to PAR readers, *Cells*, **8**, 1625, https://doi.org/10.3390/cells8121625.
7. Xie, N., Zhang, L., Gao, W., Huang, C., Huber, P. E., Zhou, X., Li, C., Shen, G., and Zou, B. (2020) NAD^+ metabolism: pathophysiologic mechanisms and therapeutic potential, *Signal Transduct. Target. Ther.*, **5**, 227, https://doi.org/10.1038/s41392-020-00311-7.
8. Amé, J. C., Rolli, V., Schreiber, V., Niedergang, C., Apiou, F., et al. (1999) PARP-2, a novel mammalian DNA damage-dependent poly(ADP-ribose) polymerase, *J. Biol. Chem.*, **274**, 17860-17868, https://doi.org/10.1074/jbc.274.25.17860.
9. Manasaryan, G., Suplatov, D., Pushkarev, S., Drobot, V., Kuimov, A., et al. (2021) Bioinformatic analysis of the nicotinamide binding site in poly(ADP-ribose) polymerase family proteins, *Cancers (Basel)*, **13**, 1201, https://doi.org/10.3390/cancers13061201.
10. Narne, P., Pandey, V., Simhadri, P. K., and Phanithi, P. B. (2017) Poly(ADP-ribose)polymerase-1 hyperactivation in neurodegenerative diseases: the death knell tolls for neurons, *Semin. Cell Dev. Biol.*, **63**, 154-166, https://doi.org/10.1016/j.semcdb.2016.11.007.
11. Henning, R. J., Bourgeois, M., and Harbison, R. D. (2018) Poly(ADP-ribose) polymerase (PARP) and PARP inhibitors: mechanisms of action and role in cardiovascular disorders, *Cardiovasc. Toxicol.*, **18**, 493-506, https://doi.org/10.1007/s12012-018-9462-2.
12. Berger, N. A., Besson, V. C., Boulares, A. H., Bürkle, A., Chiarugi, A., et al. (2018) Opportunities for the repurposing of PARP inhibitors for the therapy of non-oncological diseases, *Br. J. Pharmacol.*, **175**, 192-222, https://doi.org/10.1111/bph.13748.
13. Liu, S., Luo, W., and Wang, Y. (2022) Emerging role of PARP-1 and PARthanatos in ischemic stroke, *J. Neurochem.*, **160**, 74-87, https://doi.org/10.1111/jnc.15464.
14. Frampton, J. E. (2015) Olaparib: a review of its use as maintenance therapy in patients with ovarian cancer,

BioDrugs, **29**, 143-150, https://doi.org/10.1007/s40259-015-0125-6.

15. Mittica, G., Ghisoni, E., Giannone, G., Genta, S., Aglietta, M., Sapino, A., and Valabrega, G. (2018) PARP inhibitors in ovarian cancer, *Recent Pat. Anticancer Drug Discov.*, **13**, 392-410, https://doi.org/10.2174/1574892813666180305165256.
16. Zimmer, A. S., Gillard, M., Lipkowitz, S., and Lee, J. M. (2018) Update on PARP inhibitors in breast cancer, *Curr. Treat. Options Oncol.*, **19**, 21, https://doi.org/10.1007/s11864-018-0540-2.
17. Kirsanov, K., Fetisov, T., Antoshina, E., Trukhanova, L., Gor'kova, T., et al. (2022) Toxicological properties of 7-methylguanine, and preliminary data on its anticancer activity, *Front. Pharmacol.*, **13**, 842316, https://doi.org/10.3389/fphar.2022.842316.
18. Ruf, A., Rolli, V., de Murcia, G., and Schulz, G. E. (1998) The mechanism of the elongation and branching reaction of poly(ADP-ribose) polymerase as derived from crystal structures and mutagenesis, *J. Mol. Biol.*, **278**, 57-65, https://doi.org/10.1006/jmbi.1998.1673.
19. Gibson, B. A., and Kraus, W. L. (2012) New insights into the molecular and cellular functions of poly(ADP-ribose) and PARPs, *Nat. Rev. Mol. Cell Biol.*, **13**, 411-424, https://doi.org/10.1038/nrm3376.
20. Drenichev, M. S., and Mikhailov, S. N. (2015) Poly(ADP-ribose) - a unique natural polymer structural features, biological role and approaches to the chemical synthesis, *Nucleosides Nucleotides Nucleic Acids*, **34**, 258-276, https://doi.org/10.1080/15257770.2014.984073.
21. Alemasova, E. E., and Lavrik, O. I. (2019) Poly(ADP-ribosyl)ation by PARP1: reaction mechanism and regulatory proteins, *Nucleic Acids Res.*, **47**, 3811-3827, https://doi.org/10.1093/nar/gkz120.
22. Hoch, N. C., and Polo, L. M. (2019) ADP-ribosylation: from molecular mechanisms to human disease, *Genet. Mol. Biol.*, **43**, e20190075, https://doi.org/10.1590/1678-4685-gmb-2019-0075.
23. Brem, R., and Hall, J. (2005) XRCC1 is required for DNA single-strand break repair in human cells, *Nucleic Acids Res.*, **33**, 2512-2520, https://doi.org/10.1093/nar/gki543.
24. Ray Chaudhuri, A., and Nussenzweig, A. (2017) The multifaceted roles of PARP1 in DNA repair and chromatin remodeling, *Nat. Rev. Mol. Cell Biol.*, **18**, 610-621, https://doi.org/10.1038/nrm.2017.53.
25. Ruf, A., de Murcia, G., and Schulz, G. E. (1998) Inhibitor and NAD^+ binding to poly(ADP-ribose) polymerase as derived from crystal structures and homology modeling, *Biochemistry*, **37**, 3893-3900, https://doi.org/10.1021/bi972383s.
26. Langelier, M. F., Zandarashvili, L., Aguiar, P. M., Black, B. E., and Pascal, J. M. (2018) NAD^+ analog reveals PARP-1 substrate-blocking mechanism and allosteric communication from catalytic center to DNA-binding domains, *Nat. Commun.*, **9**, 844, https://doi.org/10.1038/s41467-018-03234-8.
27. Marsischky, G. T., Wilson, B. A., and Collier, R. J. (1995) Role of glutamic acid 988 of human poly-ADP-ribose polymerase in polymer formation. Evidence for active site similarities to the ADP-ribosylating toxins, *J. Biol. Chem.*, **270**, 3247-3254, https://doi.org/10.1074/jbc.270.7.3247.
28. Barkauskaite, E., Jankevicius, G., and Ahel, I. (2015) Structures and mechanisms of enzymes employed in the synthesis and degradation of PARP-dependent protein ADP-ribosylation, *Mol. Cell*, **58**, 935-946, https://doi.org/10.1016/j.molcel.2015.05.007.
29. Nilov, D. K., Pushkarev, S. V., Gushchina, I. V., Manasaryan, G. A., Kirsanov, K. I., and Švedas, V. K. (2020) Modeling of the enzyme-substrate complexes of human poly(ADP-ribose) polymerase 1, *Biochemistry (Moscow)*, **85**, 99-107, https://doi.org/10.1134/S0006297920010095.
30. Langelier, M. F., Planck, J. L., Roy, S., and Pascal, J. M. (2012) Structural basis for DNA damage-dependent poly(ADP-ribosyl)ation by human PARP-1, *Science*, **336**, 728-732, https://doi.org/10.1126/science.1216338.
31. Case, D. A., Belfon, K., Ben-Shalom, I. Y., Brozell, S. R., Cerutti, D. S., et al. (2020) *AMBER 2020*, University of California, San Francisco.
32. Salomon-Ferrer, R., Case, D. A., and Walker, R. C. (2013) An overview of the Amber biomolecular simulation package, *WIREs Comput. Mol. Sci.*, **3**, 198-210, https://doi.org/10.1002/wcms.1121.
33. Salomon-Ferrer, R., Götz, A. W., Poole, D., Le Grand, S., and Walker, R. C. (2013) Routine microsecond molecular dynamics simulations with AMBER on GPUs. 2. Explicit Solvent Particle Mesh Ewald, *J. Chem. Theory Comput.*, **9**, 3878-3888, https://doi.org/10.1021/ct400314y.
34. Voevodin, V. V., Antonov, A. S., Nikitenko, D. A., Shvets, P. A., Sobolev, S. I., et al. (2019) Supercomputer Lomonosov-2: large scale, deep monitoring and fine analytics for the user community, *Supercomput. Front. Innov.*, **6**, 4-11, https://doi.org/10.14529/jsfi190201.
35. Maier, J. A., Martinez, C., Kasavajhala, K., Wickstrom, L., Hause, K. E., and Simmerling, C. (2015) ff14SB: improving the accuracy of protein side chain and backbone parameters from ff99SB, *J. Chem. Theory Comput.*, **11**, 3696-3713, https://doi.org/10.1021/acs.jctc.5b00255.
36. Walker, R. C., de Souza, M. M., Mercer, I. P., Gould, I. R., and Klug, D. R. (2002) Large and fast relaxations inside a protein: calculation and measurement of reorganization energies in alcohol dehydrogenase, *J. Phys. Chem. B*, **106**, 11658-11665, https://doi.org/10.1021/jp0261814.
37. Pavelites, J. J., Gao, J., Bash, P. A., and MacKerell, A. D., Jr. (1997) A molecular mechanics force field for NAD^+, NADH, and the pyrophosphate groups

of nucleotides, *J. Comput. Chem.*, **18**, 221-239, https://doi.org/10.1002/(SICI)1096-987X(19970130)18:2<221::AID-JCC7>3.0.CO;2-X.
38. Bayly, C. I., Cieplak, P., Cornell, W. D., and Kollman, P. A. (1993) A well-behaved electrostatic potential based method using charge restraints for deriving atomic charges: the RESP model, *J. Phys. Chem.*, **97**, 10269-10280, https://doi.org/10.1021/j100142a004.
39. Dupradeau, F. Y., Pigache, A., Zaffran, T., Savineau, C., Lelong, R., et al. (2010) The R.E.D. tools: advances in RESP and ESP charge derivation and force field library building, *Phys. Chem. Chem. Phys.*, **12**, 7821-7839, https://doi.org/10.1039/c0cp00111b.
40. Nilov, D. K., Zamaraev, A. V., Zhivotovsky, B., and Kopeina, G. S. (2022) Exploring caspase mutations and post-translational modification by molecular modeling approaches, *J. Vis. Exp.*, https://doi.org/10.3791/64206-v.
41. Roe, D. R., and Cheatham, T. E., 3rd (2013) PTRAJ and CPPTRAJ: software for processing and analysis of molecular dynamics trajectory data, *J. Chem. Theory Comput.*, **9**, 3084-3095, https://doi.org/10.1021/ct400341p.
42. Humphrey, W., Dalke, A., and Schulten, K. (1996) VMD: Visual molecular dynamics, *J. Mol. Graph.*, **14**, 33-38, https://doi.org/10.1016/0263-7855(96)00018-5.
43. Walker, R. C., Crowley, M. F., and Case, D. A. (2008) The implementation of a fast and accurate QM/MM potential method in Amber, *J. Comput. Chem.*, **29**, 1019-1031, https://doi.org/10.1002/jcc.20857.
44. Stewart, J. J. (2007) Optimization of parameters for semiempirical methods V: modification of NDDO approximations and application to 70 elements, *J. Mol. Model.*, **13**, 1173-1213, https://doi.org/10.1007/s00894-007-0233-4.
45. Řezáč, J., Fanfrlík, J., Salahub, D., and Hobza, P. (2009) Semiempirical quantum chemical PM6 method augmented by dispersion and H-bonding correction terms reliably describes various types of noncovalent complexes, *J. Chem. Theory Comput.*, **5**, 1749-1760, https://doi.org/10.1021/ct9000922.
46. Barducci, A., Bussi, G., and Parrinello, M. (2008) Well-tempered metadynamics: a smoothly converging and tunable free-energy method, *Phys. Rev. Lett.*, **100**, 020603, https://doi.org/10.1103/PhysRevLett.100.020603.
47. Tribello, G. A., Bonomi, M., Branduardi, D., Camilloni, C., and Bussi, G. (2014) PLUMED 2: new feathers for an old bird, *Comput. Phys. Commun.*, **185**, 604-613, https://doi.org/10.1016/j.cpc.2013.09.018.
48. PLUMED Consortium (2019) Promoting transparency and reproducibility in enhanced molecular simulations, *Nat. Methods*, **16**, 670-673, https://doi.org/10.1038/s41592-019-0506-8.
49. Drobot, V. V., Kirilin, E. M., Kopylov, K. E., and Švedas, V. K. (2022) PLUMED plugin integration into high performance pmemd program for enhanced molecular dynamics simulations, *Supercomput. Front. Innov.*, **8**, 94-99, https://doi.org/10.14529/jsfi210408.
50. Bozdaganyan, M. E., Orekhov, P. S., Shaytan, A. K., and Shaitan, K. V. (2014) Comparative computational study of interaction of C_{60}-fullerene and tris-malonyl-C_{60}-fullerene isomers with lipid bilayer: relation to their antioxidant effect, *PLoS One*, **9**, e102487, https://doi.org/10.1371/journal.pone.0102487.
51. Raiteri, P., Laio, A., Gervasio, F. L., Micheletti, C., and Parrinello, M. (2006) Efficient reconstruction of complex free energy landscapes by multiple walkers metadynamics, *J. Phys. Chem. B*, **110**, 3533-3539, https://doi.org/10.1021/jp054359r.
52. Trapl, D., and Spiwok, V. (2022) Analysis of the results of metadynamics simulations by metadynminer and metadynminer3d, *R J.*, **14**, 46-58, https://doi.org/10.32614/RJ-2022-057.
53. Henkelman, G., and Jónsson, H. (2000) Improved tangent estimate in the nudged elastic band method for finding minimum energy paths and saddle points, *J. Chem. Phys.*, **113**, 9978-9985, https://doi.org/10.1063/1.1323224.
54. Zlobin, A., and Golovin, A. (2022) Between protein fold and nucleophile identity: multiscale modeling of the TEV protease enzyme-substrate complex, *ACS Omega*, **7**, 40279-40292, https://doi.org/10.1021/acsomega.2c05201.
55. Kopylov, K., Kirilin, E., and Švedas, V. (2023) Conformational transitions induced by NADH binding promote reduction half-reaction in 2-hydroxybiphenyl-3-monooxygenase catalytic cycle, *Biochem. Biophys. Res. Commun.*, **639**, 77-83, https://doi.org/10.1016/j.bbrc.2022.11.066.
56. Calvelo, M., Males, A., Alteen, M. G., Willems, L. I., Vocadlo, et al. (2023) Human *O*-GlcNAcase uses a preactivated boat-skew substrate conformation for catalysis. Evidence from X-ray crystallography and QM/MM metadynamics, *ACS Catal.*, **13**, 13672-13678, https://doi.org/10.1021/acscatal.3c02378.
57. Corbeski, I., Vargas-Rosales, P. A., Bedi, R. K., Deng, J., Coelho, D., et al. (2024) The catalytic mechanism of the RNA methyltransferase METTL3, *Elife*, **12**, RP92537, https://doi.org/10.7554/eLife.92537.
58. Khrenova, M. G., Nikiforov, A. A., Andrijchenko, N. N., Mironov, V. A., and Nemukhin, A. V. (2014) The photoreaction mechanism in the bacterial blue light receptor BLUF according to metadynamics modeling, *Moscow Univ. Chem. Bull.*, **69**, 149-151, https://doi.org/10.3103/S0027131414040038.
59. Wang, Y., Rösner, D., Grzywa, M., and Marx, A. (2014) Chain-terminating and clickable NAD^+ analogues for labeling the target proteins of ADP-ribosyltransferases, *Angew. Chem. Int. Ed. Engl.*, **53**, 8159-8162, https://doi.org/10.1002/anie.201404431.